



## Article

# Quantum Cutting in $\text{KGd}(\text{CO}_3)_2:\text{Tb}^{3+}$ Green Phosphor

Dechuan Li <sup>1,2,\*</sup>, Jian Qian <sup>1,2</sup>, Lei Huang <sup>1,2</sup>, Yumeng Zhang <sup>1,2</sup> and Guangping Zhu <sup>1,2</sup><sup>1</sup> School of Physics and Electronic Information, Huaibei Normal University, Huaibei 235000, China<sup>2</sup> Key Laboratory of Green and Precise Synthetic Chemistry and Applications, Ministry of Education, Huaibei 235000, China

\* Correspondence: lidechuan@chnu.edu.cn

**Abstract:** Phosphors with a longer excitation wavelength exhibit higher energy conversion efficiency. Herein, quantum cutting  $\text{KGd}(\text{CO}_3)_2:\text{Tb}^{3+}$  phosphors excited by middle-wave ultraviolet were synthesized via a hydrothermal method. All the  $\text{KGd}(\text{CO}_3)_2:x\text{Tb}^{3+}$  phosphors remain in monoclinic structures in a large  $\text{Tb}^{3+}$  doping range. In the  $\text{KGd}(\text{CO}_3)_2$  host,  ${}^6\text{D}_{3/2}$  and  ${}^6\text{I}_{17/2}$  of  $\text{Gd}^{3+}$  were employed for quantum cutting in sensitizing levels. The excited state electrons could easily transfer from  $\text{Gd}^{3+}$  to  $\text{Tb}^{3+}$  with high efficiency. There are three efficient excited bands for quantum cutting. The excited wavelengths of 244, 273, and 283 nm correspond to the transition processes of  ${}^8\text{S}_{7/2}\rightarrow{}^6\text{D}_{3/2}$  ( $\text{Gd}^{3+}$ ),  ${}^8\text{S}_{7/2}\rightarrow{}^6\text{I}_{17/2}$  ( $\text{Gd}^{3+}$ ), and  ${}^7\text{F}_6\rightarrow{}^5\text{F}_4$  ( $\text{Tb}^{3+}$ ), and the maximum quantum yields of  $\text{KGd}(\text{CO}_3)_2:\text{Tb}^{3+}$  can reach 163.5, 119, and 143%, respectively. The continuous and efficient excitation band of 273–283 nm can well match the commercial 275 nm LED chip to expand the usage of solid-state light sources. Meanwhile, the phosphor also shows good excitation efficiency at 365 nm in a high  $\text{Tb}^{3+}$  doping concentration. Therefore,  $\text{KGd}(\text{CO}_3)_2:\text{Tb}^{3+}$  is an efficient green-emitting phosphor for ultraviolet-excited solid-state light sources.

**Keywords:**  $\text{Gd}^{3+}$ ;  $\text{Tb}^{3+}$ ; quantum cutting; phosphor

## 1. Introduction

$\text{Gd}^{3+}$ , one of the most popular ions, was used to sensitize  $\text{Tb}^{3+}$  [1–4],  $\text{Eu}^{3+}$  [5,6],  $\text{Dy}^{3+}$  [7,8], and  $\text{Sm}^{3+}$  [9,10] in luminescence emission. There are four excited energy bands,  ${}^6\text{G}_J$ ,  ${}^6\text{D}_J$ ,  ${}^6\text{I}_J$ , and  ${}^6\text{P}_J$ , below  $5200\text{ cm}^{-1}$  in a  $\text{Gd}^{3+}$  ion [11]. Energy level matching enables excited electrons to transfer between different excited states by resonance, cross-relaxation, and phonon assistance [9,12]. The higher the energy of the exciting light, the greater the possibility of the energy level matching. In much of the literature, vacuum ultraviolet and short-wave ultraviolet are widely used for efficient quantum cutting [4,13]. In the energy range of  $4500\text{--}5200\text{ cm}^{-1}$ , the higher energy band is ascribed to  $\text{Gd}^{3+}$  absorption of the  ${}^6\text{G}_J$  multiplet, which corresponds to the excitation light of vacuum or short-wave ultraviolet. Efficient emission of quantum cutting can be easily achieved with the assistance of  ${}^6\text{G}_J$  [13–18]. When the excited state energy is lower than  $3900\text{ cm}^{-1}$ , energy level matching is difficult to achieve for quantum cutting. Some of the literature describes quantum cutting assisted with the  ${}^6\text{D}_J$  and  ${}^6\text{I}_J$  energy bands in the  $\text{Tb}^{3+}$  emission. However, excited state ions can easily transfer from  $\text{Gd}^{3+}$  to  $\text{Eu}^{3+}$  and  $\text{Dy}^{3+}$  by nonradiative relation and energy transfer in the  ${}^6\text{D}_J$  and  ${}^6\text{I}_J$  energy bands [19,20]. Additionally, the  ${}^6\text{I}_J$  energy band consists of six energy levels:  ${}^6\text{I}_{15/2}$  ( $36,725\text{ cm}^{-1}$ ),  ${}^6\text{I}_{13/2}$  ( $36,711\text{ cm}^{-1}$ ),  ${}^6\text{I}_{11/2}$  ( $36,525\text{ cm}^{-1}$ ),  ${}^6\text{I}_{17/2}$  ( $36,461\text{ cm}^{-1}$ ),  ${}^6\text{I}_{9/2}$  ( $36,231\text{ cm}^{-1}$ ), and  ${}^6\text{I}_{7/2}$  ( $35,878\text{ cm}^{-1}$ ), which correspond to the theoretical excitation wavelengths of 272.4, 272.5, 273.9, 274.4, 276.1, and 278.8 nm in  $\text{Gd}^{3+}$  [11], respectively. The  $\text{Gd}^{3+}$  absorption of the  ${}^6\text{I}_J$  level matches well with the 275 nm LED solid-state light source, which can be used to break through the limitation of the mercury lamp for miniaturization and portability of the product.

Rare earth carbonate is an excellent optical material with high photoluminescence [21,22] and birefringence [23,24]. In this work, we reported on the quantum cutting of  $\text{Gd}^{3+}$  sensi-



**Citation:** Li, D.; Qian, J.; Huang, L.; Zhang, Y.; Zhu, G. Quantum Cutting in  $\text{KGd}(\text{CO}_3)_2:\text{Tb}^{3+}$  Green Phosphor. *Nanomaterials* **2023**, *13*, 351. <https://doi.org/10.3390/nano13020351>

Academic Editor: Seung Hwan Ko

Received: 13 December 2022

Revised: 5 January 2023

Accepted: 13 January 2023

Published: 15 January 2023



**Copyright:** © 2023 by the authors. Licensee MDPI, Basel, Switzerland. This article is an open access article distributed under the terms and conditions of the Creative Commons Attribution (CC BY) license (<https://creativecommons.org/licenses/by/4.0/>).

tized  $\text{KGd}(\text{CO}_3)_2:\text{Tb}^{3+}$  phosphor in a relatively lower level of  ${}^6\text{D}_J$  and  ${}^6\text{I}_J$ . In the phosphor, three important quantum cutting levels,  ${}^6\text{I}_J$  ( $\text{Gd}^{3+}$ ),  ${}^6\text{D}_J$  ( $\text{Gd}^{3+}$ ), and  ${}^5\text{F}_J$  ( $\text{Tb}^{3+}$ ), were systematically studied by the luminescence spectra, quantum yields, and decay curves. The detailed transfer processes of excited electrons between different energy levels are discussed.

## 2. Materials and Methods

$\text{KGd}_{1-x}(\text{CO}_3)_2:x\text{Tb}^{3+}$  ( $x = 0, 0.005, 0.05, 0.1, 0.3, 0.5, 0.7, 0.9$ , note as  $\text{KGdC}:x\text{Tb}^{3+}$ ) phosphors were synthesized via a hydrothermal method with the raw materials  $\text{Gd}(\text{NO}_3)_3 \cdot 6\text{H}_2\text{O}$  (99.99%) and  $\text{Tb}(\text{NO}_3)_3 \cdot 6\text{H}_2\text{O}$  (99.99%). First, the nitrates of  $\text{Gd}(\text{NO}_3)_3$  and  $\text{Tb}(\text{NO}_3)_3$  were dissolved into deionized water. Second, the mixture was added to the  $\text{K}_2\text{CO}_3$  solution (0.55 mol/L) under vigorous stirring. Third, diluted nitric acid was used to adjust the pH value (9.5) of the mixture solution. Finally, the reaction solution was transferred to an autoclave and heated at  $200^\circ\text{C}$  for 8 h. Then, the precipitate was washed with deionized water and ethanol three times. The phosphor was dried at  $60^\circ\text{C}$  (40 min) for the final product.

The crystal structures of  $\text{KGd}(\text{CO}_3)_2:x\text{Tb}^{3+}$  were analyzed by the X-ray diffractometer in the range of  $10\text{--}80^\circ$  (PANalytical, Almelo, the Netherlands). The morphologies and energy dispersive spectrum (EDS) were imaged via cold field emission scanning electron microscopy (Regulus 8220, Hitachi High-Tech Co., Tokyo, Japan). The luminescent properties were measured by an FLS920 fluorescence spectrophotometer equipped with 450 W Xe-lamp (Edinburgh Instruments, Livingston, UK). Using  $\text{BaSO}_4$  as a reference, powder samples were placed in the PTFE powder vessels and slotted into the sample holder, and then the absolute quantum yields were measured by the integrating sphere within the FLS920 sample chamber in an indirect method. The lifetimes of  $\text{KGd}(\text{CO}_3)_2:x\text{Tb}^{3+}$  were tested by the 60 W microsecond flashlamp (Edinburgh Instruments, Livingston, UK).

## 3. Results and Discussion

### 3.1. Crystal Structures

Figure 1 shows the diffraction patterns of  $\text{Tb}^{3+}$ -doped  $\text{KGdC}$  at  $x = 0.1$  and  $0.9$ . In the variation in  $\text{Tb}^{3+}$  doping concentration, the diffraction peaks of samples are almost the same. The crystal structures remain stable in a larger  $\text{Tb}^{3+}$  doping range. The most intense diffraction peak is located at the (110) crystal plane for all samples. All the diffraction patterns are consistent with the standard card of monoclinic  $\text{KGd}(\text{CO}_3)_2$  (JCPDS:1-88-1422) [25]. As the  $\text{Tb}^{3+}$  concentration increased, the diffraction peak of the (110) crystal plane shifted to a large angle. With a similar ion radius,  $\text{Gd}^{3+}$  (1.05 Å) could be easily substituted by  $\text{Tb}^{3+}$  (1.04 Å) at an arbitrary proportion [26]. Pure phase  $\text{KGdC}:x\text{Tb}^{3+}$  phosphors were successfully synthesized without any second phase.

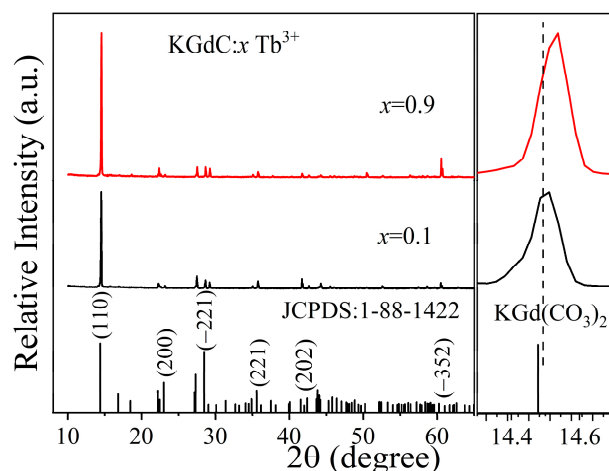


**Figure 1.** X-ray diffraction patterns of  $\text{KGdC}:x\text{Tb}^{3+}$  ( $x = 0.1, 0.9$ ).

### 3.2. Morphology

Figure 2 shows the morphologies of KGdC: $x$ Tb $^{3+}$  with different Tb $^{3+}$  doping concentrations. As shown in Figure 2a–f, most of the particles exhibit well-developed monoclinic crystal grains with a size of about 80–350  $\mu$ m. When the Tb $^{3+}$  doping concentration is increased, the morphology of grains changes slightly. All grains show good monoclinic structure in samples with different Tb $^{3+}$  doping ratios. The size of monoclinic grains is relatively large, especially at  $x = 0.3$ . Although large grains are easy to fracture, the type of grains could be clearly identified. A small area of monoclinic grain was selected to demonstrate the existence of elements in KGdC:0.5Tb $^{3+}$ . In the element distribution maps, K, Gd and Tb were well-dispersed (Figure 2g–i). As shown in Figure 2j, the element content was similar to the original stoichiometric ratio.

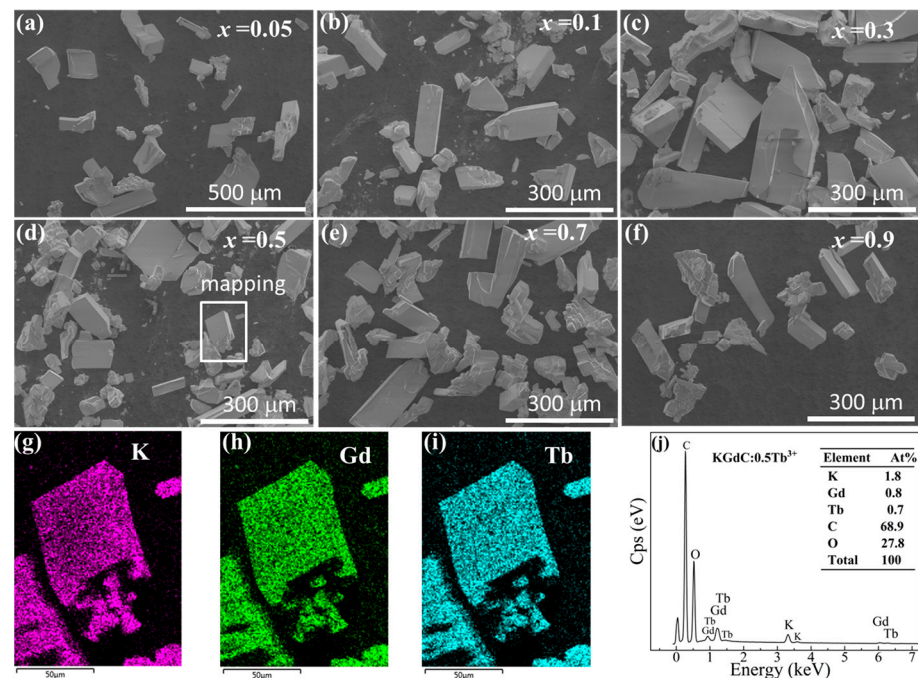


**Figure 2.** (a–f) Morphologies of KGdC: $x$ Tb $^{3+}$  ( $x = 0.05, 0.1, 0.3, 0.5, 0.7, 0.9$ ); (g–i) Elemental mapping of K, Gd, and Tb; (j) Energy dispersive spectroscopy analysis.

### 3.3. Luminescence Spectra

In the low Tb $^{3+}$  doping concentration, the interactions between the emission ions are weak, and the transfer process of the excited state electrons is easily traced. Figure 3 shows the luminescence properties of KGdC: $x$ Tb $^{3+}$  at  $x = 0.005$ . The efficiently excited wavelengths are clearly shown in Figure 3a for the 542 nm emission. On the excitation spectrum, the intense excitation peaks are located at 244, 253, 273, 306, and 312 nm, corresponding to the Gd $^{3+}$  transitions from  $^8S_{7/2}$  ground state to  $^6D_{3/2}$ ,  $^6D_{9/2}$ ,  $^6I_{17/2}$ ,  $^6P_{5/2}$ , and  $^6P_{7/2}$  excited states [11], respectively. Additionally, the weak excitation peaks are located at 351, 368, and 376 nm, corresponding to the Tb $^{3+}$  transitions from  $^7F_6$  to  $^5L_9$ ,  $^5L_{10}$ , and  $^5G_6$  [27,28], respectively. However, the intense peaks of the entire exciting spectrum mainly consist in the absorption of Gd $^{3+}$ , which indicates a high transfer efficiency from Gd $^{3+}$  to Tb $^{3+}$ . The contribution of Gd $^{3+}$  is indicated by the emission spectra in Figure 3b. Under the excitations of 244, 253, 273, and 306 nm, most of the Gd $^{3+}$  excited state electrons could transfer to Tb $^{3+}$  with the typical luminescence emission of 542 nm. Another typical emission of Gd $^{3+}$  at 312 nm could be observed in all spectra, which indicates that a fraction of high excited state electrons could depopulate to ground state through the  $^6P_{7/2}$  intermediate excited state.

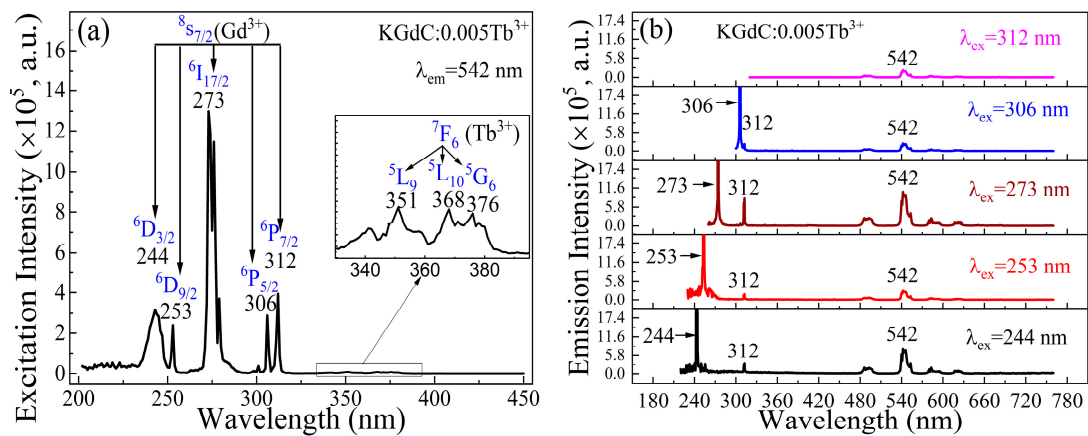


**Figure 3.** Luminescence properties of KGdC:0.005Tb<sup>3+</sup>: (a) Excitation spectrum; (b) Emission spectra excited at 244, 253, 273, 306, and 312 nm.

As shown in Figure 4a, the peak intensities at 273 nm decreased rapidly with the increasing Tb<sup>3+</sup> concentration in KGdC:*x*Tb<sup>3+</sup> phosphor monitored at 312 nm. The excitation intensities at 244, 253, and 273 nm are intense in low Tb<sup>3+</sup> doping. When *x* is larger than 0.005, the excited intensities at 244 and 253 nm almost disappear. Furthermore, the exciting intensity at 273 nm also decreases rapidly. The excited intensity quenching of Gd<sup>3+</sup> indicates that most excited state electrons cannot release energy through Gd<sup>3+</sup> itself in a 312 nm emission at a high Tb<sup>3+</sup> concentration.

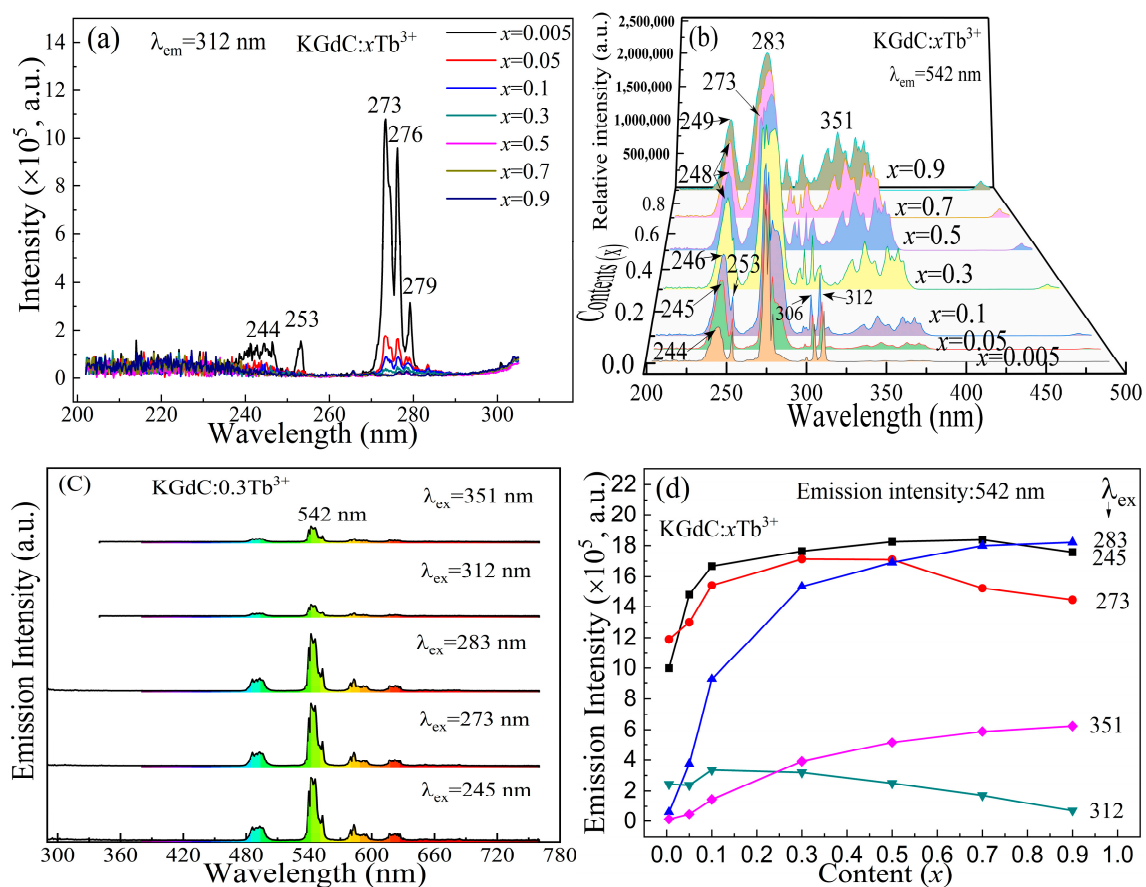


**Figure 4.** Luminescence properties of KGdC:*x*Tb<sup>3+</sup> (a) Excited spectra monitored at 312 nm; (b) Excited spectra monitored at 542 nm; (c) Typical emission spectra of KGdC:0.3Tb<sup>3+</sup> at different exciting wavelengths; (d) 542 nm emission intensities.

Figure 4b shows the variations in exciting spectra under different Tb<sup>3+</sup> concentrations in KGdC:xTb<sup>3+</sup> phosphor monitored at 542 nm. At the lowest Tb<sup>3+</sup> doping, the contribution to the Tb<sup>3+</sup> emission is effective, with the intense absorption peaks of Gd<sup>3+</sup> at 244, 253, 273, 306, and 312 nm. When the Tb<sup>3+</sup> doping concentration is increased, the exciting peaks of short wavelength are slightly shifted to the longer wavelength from 244 to 249 nm, corresponding to the Tb<sup>3+</sup> spin-allowed transition [29,30]. The other excitation peaks remain in the same position except for the variation in excitation intensity. The most obvious change is that the excitation intensities at 283 nm increased with the Tb<sup>3+</sup> concentration, which corresponded to the abolishment of the Tb<sup>3+</sup> spin-forbidden transition [22]. In the range of 300–380 nm, the exciting peaks were related to the f–f transition of Tb<sup>3+</sup> [30]. Two excitation bands show strong absorption at high Tb<sup>3+</sup> concentrations, which is suitable for the excitation of commercial 275 and 365 nm UV LED.

The typical emission intensities of KGdC:0.3Tb<sup>3+</sup> at different excitation wavelengths are shown in Figure 4c. In the emission spectra of KGdC:0.3Tb<sup>3+</sup>, the 312 nm emission peak almost disappears for the excitation at 245, 273, and 283 nm. Meanwhile, the efficient emission intensities at 542 nm are about four times higher than those excited at 312 and 351 nm at x = 0.3. The relative emission intensities of KGdC:xTb<sup>3+</sup> at 542 nm are shown in Figure 4d. As seen in the curves, the emission intensities at 245, 273, and 283 nm are relatively high. Especially for 245 nm excitation, the medium intensity of exciting light emitted the strongest emission light, which indicated that a higher efficient transfer existed between Gd<sup>3+</sup> and Tb<sup>3+</sup>. For the excitation wavelengths of 273 and 283 nm, the phosphors exhibited a higher emission intensity in a wide range of Tb<sup>3+</sup> doping. Moreover, the excitation spectrum of the phosphor is continuous in the range of 273 to 283 nm, which effectively matches the excitation of the 275 nm LED. For the excitation wavelength at 351 nm, the green emission intensity of phosphors slightly increased with increasing concentrations of Tb<sup>3+</sup> ions without any concentration quenching. In addition, the decrease in emission intensity excited at 312 nm indicates that there is concentration quenching at this energy level in a high Tb<sup>3+</sup> doping concentration.

### 3.4. Energy Level Diagram

Figure 5 shows the energy level diagram for the transitions of excited state electrons in the emission process. First, 244 nm photons are absorbed by Gd<sup>3+</sup> in the <sup>8</sup>S<sub>7/2</sub>→<sup>6</sup>D<sub>3/2</sub> transition [31]. One of the excited state electrons in <sup>6</sup>D<sub>3/2</sub> depopulates to <sup>6</sup>P<sub>7/2</sub> in a non-radiation way; then, the electrons continually transfer to the <sup>8</sup>S<sub>7/2</sub> ground state, and emit 312 nm photons. Owing to the similar energy levels of 40,851 cm<sup>-1</sup> (Gd<sup>3+</sup>, <sup>6</sup>D<sub>3/2</sub>) [11] and 40,749 cm<sup>-1</sup> (Tb<sup>3+</sup>, <sup>5</sup>K<sub>8</sub>) [27], the other parts of the excited state electron transfer to the neighboring Tb<sup>3+</sup> by resonance vibration. Then, the cross-relaxation occurs between two Tb<sup>3+</sup>: <sup>5</sup>K<sub>8</sub> + <sup>7</sup>F<sub>6</sub>→<sup>5</sup>D<sub>4</sub> + <sup>5</sup>D<sub>4</sub> (process 1) [21]. Finally, two excited state electrons in <sup>5</sup>D<sub>4</sub> are stimulated by one excited photon for the quantum cutting of <sup>5</sup>D<sub>4</sub>→<sup>7</sup>F<sub>J</sub> (J = 6, 5, 4, 3) with typical Tb<sup>3+</sup> emission at 542 nm.

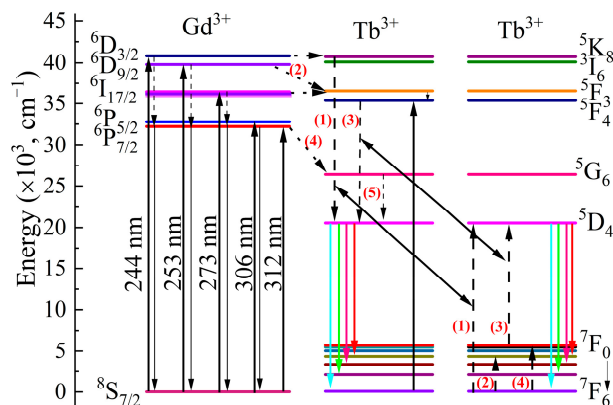


Figure 5. Energy level diagram of KGdC:Tb<sup>3+</sup>.

In the excitation of 253, 273, and 306 nm, the ground state electrons of  $Gd^{3+}$  are excited to  ${}^6D_{9/2}$ ,  ${}^6I_{17/2}$ , and  ${}^6P_{5/2}$  levels, respectively. One of the excited electrons returns to the  ${}^6P_{7/2}$  in a non-radiation way for the 312 nm emission. Most excited state electrons are transferred to  $Tb^{3+}$  with high transfer efficiency [32]. The similar energy gaps of  ${}^6D_{9/2}$ - ${}^5F_3$  ( $3200\text{ cm}^{-1}$ ) and  ${}^7F_6$ - ${}^7F_3$  ( $3270\text{ cm}^{-1}$ ) are beneficial to the  ${}^6D_{9/2}$  electronic cross relation for the accumulation of  ${}^5F_3$  excited state electron populations in process 2 [27]. Meanwhile,  ${}^6I_{17/2}$  ( $Gd^{3+}$ ) excited state electrons also transfer to the adjacent  ${}^5F_3$  ( $Tb^{3+}$ ) level by resonance migration. Then,  ${}^5F_3$  excited state electrons relax to the  ${}^5F_4$  level. In process 3, the energy gaps between  ${}^5F_4$ - ${}^5D_4$  ( $14,835\text{ cm}^{-1}$ ) and  ${}^7F_0$ - ${}^5D_4$  ( $14,842\text{ cm}^{-1}$ ) are close enough for the cross-relation:  ${}^5F_4 + {}^7F_6 \rightarrow {}^5D_4 + {}^5D_4$  [27]. This is also another effective way to realize quantum cutting in KGdC: $xTb^{3+}$  phosphor. As for the  $Gd^{3+}$ , the excited state electrons in  ${}^6P_{7/2}$  reach the  ${}^5D_4$  level of  $Tb^{3+}$  by cross-relaxation and non-radiation transition in processes 4 and 5. Another exciting peak at 283 nm is attributed to the  $Tb^{3+}$  absorption from  ${}^7F_6$  to  ${}^5F_4$ . The excited state electrons are directly transferred to the  ${}^5D_4$  level by cross-relaxation for the two-photon emission.

### 3.5. Quantum Yield

Figure 6 shows the quantum yields (QY) of KGdC: $xTb^{3+}$  ( $x = 0.05, 0.1, 0.3, 0.5, 0.7, 0.9$ ) under different excitation wavelengths. The results show that there are three efficient excitation bands in the quantum cutting process of KGdC: $xTb^{3+}$ . On the top curve, the initial value of QY reaches 132% at  $x = 0.05$  under the 245 nm excitation. Moreover, under the optimal excitation wavelength, all QY values of KGdC: $xTb^{3+}$  are greater than 100% and the maximum value is 163.5% at  $x = 0.5$ . This QY value is close to those of  $Tb^{3+}$ -doped  $Ca_9Y(PO_4)_7$  (157%) [4],  $K_2GdF_5$  (177%) [33], and  $KY(CO_3)_2$  (177%) [22]. On the middle and lower curves, the exciting efficiency at 273 nm is greater than that at 283 nm only at  $x = 0.05$ . Quantum yields are greater than 100% in the  $Tb^{3+}$  doping range of 0.3–0.7. As for KGdC:0.5 $Tb^{3+}$ , the maximum QYs are 119 and 143% under the excitations at 273 and 283 nm, respectively. In addition, the series of weak excitation peaks caused by the f-f transition of  $Tb^{3+}$  ions is also worthy of discussion. In the range of 320–390 nm, 351 nm is the typical excitation wavelength for  $Tb^{3+}$  emission. QY values increase with the increasing  $Tb^{3+}$  doping concentration. Compared with the other luminescent hosts, phosphate [34], fluoroborates [35], and silicate [36], concentration quenching does not occur in the KGC host with a high  $Tb^{3+}$  doping concentration. The unique structure of  $[REO_8]$  polyhedral enables the sufficient distance between adjacent  $Tb^{3+}$  to avoid energy loss [21,23]. The maximum QY was 91.44% for KGdC:0.9 $Tb^{3+}$ . It is interesting to confirm that the highly efficient excitation bands of quantum cutting are broad in KGdC host material, which is beneficial for choosing an appropriate exciting source for the application of solid-state lighting [37].

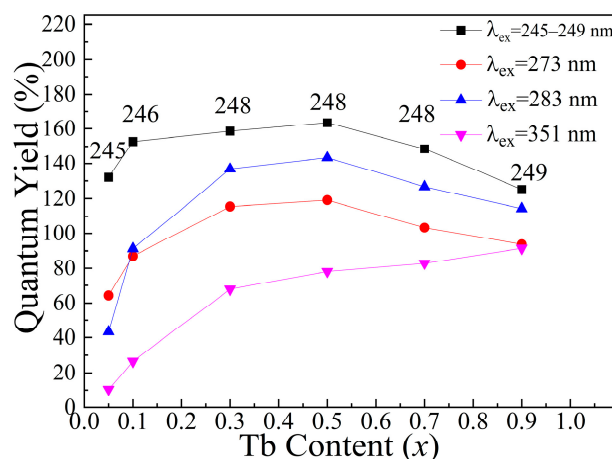


Figure 6. Quantum Yields of KGdC: $xTb^{3+}$  under different excitation wavelengths.

### 3.6. Decay Curve

Figure 7a shows the decay curves of KGdC: $x$ Tb $^{3+}$  under excitation at 273 nm. The electronic depopulation of the  $^5D_4$  level is characterized by the decay curve. As shown in the figure, all decay curves could be fitted by the single exponential. The fitted lifetimes mainly originate from the decay process of excited state electrons at the  $^5D_4$  level. The values of a lifetime were shown in Figure 7b. In the excitation at 273 nm, the lifetime values of the  $^5D_4$  level first increase and then decrease with an increasing Tb $^{3+}$  concentration. The dramatic change originates from the competition between the  $^6I_{17/2}$  (Gd $^{3+}$ ) and  $^5F_3$  (Tb $^{3+}$ ) levels. The lifetime value is small in a small number of Tb $^{3+}$ . When the Tb $^{3+}$  doping concentration is increased, the energy transfers between Gd $^{3+}$  and Tb $^{3+}$  are efficiently enhanced [38]. The lifetimes increase with the increasing number of excited state electrons. When  $x$  is larger than 0.3, the high concentration of Tb $^{3+}$  improves the cross-relaxation efficiency between two Tb $^{3+}$ . The rapid accumulation of excited state electrons decreases the energy lifetime of the  $^5D_4$  level. As for the excitation at 245 and 283 nm, there are two lower excitation intensities for the 312 nm emissions than that of 273 nm in low Tb $^{3+}$  doping concentration (as shown in Figure 4a). The competition of excited state electrons between Gd $^{3+}$  and Tb $^{3+}$  is weak. The Gd $^{3+}$  emission consumes a small number of excited state electrons, which results in a slight reduction in lifetime. When the Tb $^{3+}$  doping concentration is further increased, the lifetime decreases rapidly in a shortened distance between Tb $^{3+}$  ions [39].

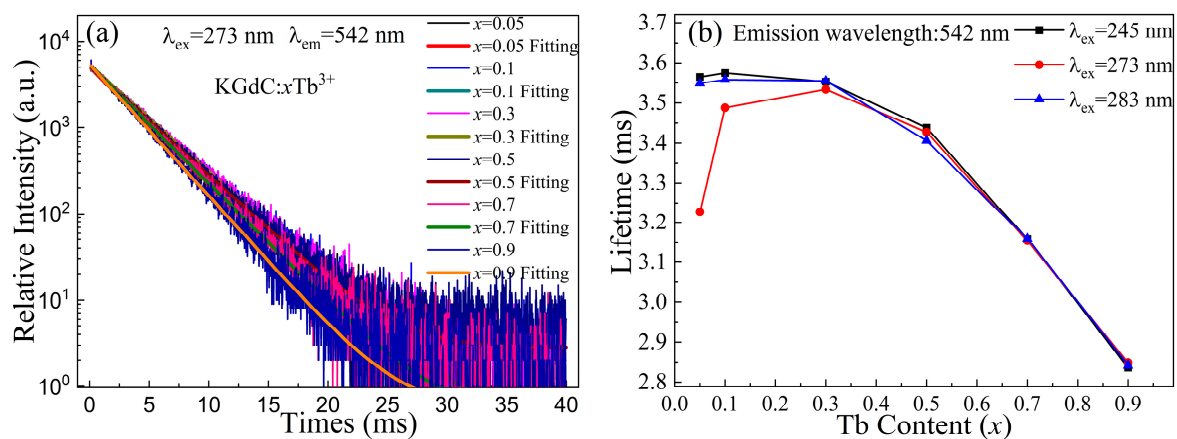


Figure 7. Decay properties of KGdC: $x$ Tb $^{3+}$  (a) decay curves; (b) Lifetimes of Tb $^{3+}$   $^5D_4$  level.

## 4. Conclusions

Tb $^{3+}$ -doped KGd(CO $_3$ ) $_2$  phosphors with high quantum yields were prepared via a hydrothermal method. Tb $^{3+}$  could substitute for Gd $^{3+}$  in the KGd(CO $_3$ ) $_2$  crystal lattice at any proportion. In the Tb $^{3+}$ -doped KGd(CO $_3$ ) $_2$  material, Gd $^{3+}$  is both an activated and sensitized ion. The energy transfer between Gd $^{3+}$  and Tb $^{3+}$  is highly efficient. Quantum cutting can be effectively triggered at three excitation bands: 245, 273, and 283 nm. Under excitation at 245 nm, the quantum yield of KGdC: $x$ Tb $^{3+}$  phosphor could reach 132% at  $x = 0.05$ , and the maximal value is 163.5% in the quantum cutting process of KGdC:0.5Tb $^{3+}$ . The excitation bands at 273 and 283 nm are continuous, which is consistent with the emission wavelength of commercial 275 nm LED. The highly efficient KGdC:Tb $^{3+}$  phosphor could be potentially applied to the ultraviolet-excited solid-state light sources.

**Author Contributions:** Conceptualization, D.L. and G.Z.; investigation, D.L. and Y.Z.; resources, D.L., J.Q. and L.H.; data curation, J.Q. and L.H.; writing—original draft preparation, D.L.; writing—review and editing, D.L.; visualization, D.L.; supervision, D.L.; project administration, D.L.; funding acquisition, D.L. and Y.Z. All authors have read and agreed to the published version of the manuscript.

**Funding:** This research was funded by the University Natural Science Research Project of Anhui Province (KJ2020A0048) and Anhui Natural Science Foundation (2108085QA30).

**Data Availability Statement:** Not applicable.

**Acknowledgments:** The authors would like to acknowledge financial support from the University Natural Science Research Project of Anhui Province and the Anhui Natural Science Foundation.

**Conflicts of Interest:** The authors declare no conflict of interest.

## References

1. Bao, S.; Yu, H.; Gao, G.; Zhu, H.; Wang, D.; Zhu, P.; Wang, G. Rare-earth single atom based luminescent composite nanomaterials: Tunable full-color single phosphor and applications in WLEDs. *Nano Res.* **2022**, *15*, 3594–3605. [[CrossRef](#)]
2. Van Do, P.; Quang, V.X.; Thanh, L.D.; Tuyen, V.P.; Ca, N.X.; Hoa, V.X.; Van Tuyen, H. Energy transfer and white light emission of KGdF<sub>4</sub> polycrystalline co-doped with Tb<sup>3+</sup>/Sm<sup>3+</sup> ions. *Opt. Mater.* **2019**, *92*, 174–180. [[CrossRef](#)]
3. Jaiswal, S.R.; Nagpure, P.A.; Omanwar, S.K. Improvement of quantum efficiency through Gd<sup>3+</sup> to Eu<sup>3+</sup> energy transfer in YF<sub>3</sub> phosphor. *Luminescence* **2021**, *36*, 1395–1401. [[CrossRef](#)] [[PubMed](#)]
4. Zhang, F.; Xie, J.; Li, G.; Zhang, W.; Wang, Y.; Huang, Y.; Tao, Y. Cation composition sensitive visible quantum cutting behavior of high efficiency green phosphors Ca<sub>9</sub>Ln(PO<sub>4</sub>)<sub>7</sub>:Tb<sup>3+</sup> (Ln = Y, La, Gd). *J. Mater. Chem. C* **2017**, *5*, 872–881. [[CrossRef](#)]
5. Ramakrishna, P.; Padhi, R.K.; Mohapatra, D.K.; Jena, H.; Panigrahi, B.S. Structural characterization, Gd<sup>3+</sup>→Eu<sup>3+</sup> energy transfer and radiative properties of Gd/Eu in codoped Li<sub>2</sub>O–ZnO–SrO–B<sub>2</sub>O<sub>3</sub>–P<sub>2</sub>O<sub>5</sub> glass. *Opt. Mater.* **2022**, *125*, 112060. [[CrossRef](#)]
6. Zhong, Y.; Wu, Q.; Zhu, J.; Cai, P.; Du, P. Room-Temperature Synthesis of Highly-Efficient Eu<sup>3+</sup>-Activated KGd<sub>2</sub>F<sub>7</sub> Red-Emitting Nanoparticles for White Light-Emitting Diode. *Nanomaterials* **2022**, *12*, 4397. [[CrossRef](#)]
7. Xu, Z.; Zhu, Q.; Li, X.; Sun, X.; Li, J.-G. White-light emitting (Y,Gd)PO<sub>4</sub>:Dy<sup>3+</sup> microspheres: Gd<sup>3+</sup> mediated morphology tailoring and selective energy transfer and correlation of photoluminescence behaviors. *Mater. Res. Bull.* **2019**, *110*, 149–158. [[CrossRef](#)]
8. Ye, W.; Wang, Y.; Zhao, C.; Wen, Z.; Cao, Z.; Cao, Z.; Shen, X.; Li, Y.; Yuan, X.; Wang, C.; et al. Optical temperature sensing based on phonon-assisted population of Dy<sup>3+</sup> sensitized by Gd<sup>3+</sup> in Gd<sub>2</sub>Ge<sub>2</sub>O<sub>7</sub> nanophosphors. *J. Lumin.* **2020**, *227*, 117567. [[CrossRef](#)]
9. Gupta, P.; Bedyal, A.K.; Kumar, V.; Khajuria, Y.; Sharma, V.; Ntwaeaborwa, O.M.; Swart, H.C. Energy transfer mechanism from Gd<sup>3+</sup> to Sm<sup>3+</sup> in K<sub>3</sub>Gd(PO<sub>4</sub>)<sub>2</sub>:Sm<sup>3+</sup> phosphor. *Mater. Res. Express* **2015**, *2*, 076202. [[CrossRef](#)]
10. Wantana, N.; Kaewjaeng, S.; Kothan, S.; Kim, H.J.; Kaewkhao, J. Energy transfer from Gd<sup>3+</sup> to Sm<sup>3+</sup> and luminescence characteristics of CaO–Gd<sub>2</sub>O<sub>3</sub>–SiO<sub>2</sub>–B<sub>2</sub>O<sub>3</sub> scintillating glasses. *J. Lumin.* **2017**, *181*, 382–386. [[CrossRef](#)]
11. Carnall, W.; Fields, P.; Rajnak, K. Electronic Energy Levels of the Trivalent Lanthanide Aquo Ions. II. Gd<sup>3+</sup>. *J. Chem. Phys.* **1968**, *49*, 4443–4446. [[CrossRef](#)]
12. Selvalakshmi, T.; Bose, A.C.; Velmathi, S. Effect of Eu<sup>3+</sup> and Al<sup>3+</sup> Concentrations on Photoluminescence of Gd<sub>2</sub>O<sub>3</sub>:Eu<sup>3+</sup>. *J. Nanosci. Nanotechnol.* **2015**, *15*, 5760–5767. [[CrossRef](#)] [[PubMed](#)]
13. Jaiswal, S.; Nagpure, P.; Omanwar, S. Energy Transfer Process in MgF<sub>2</sub>:Gd<sup>3+</sup>,Eu<sup>3+</sup> Phosphor: Application to Visible Quantum Cutting. *Int. J. Sci. Res. Sci. Technol.* **2021**, *8*, 272–276.
14. Liang, W.; Wang, Y. Visible quantum cutting through downconversion in Eu<sup>3+</sup>-doped K<sub>2</sub>GdZr(PO<sub>4</sub>)<sub>3</sub> phosphor. *Mater. Chem. Phys.* **2010**, *119*, 214–217. [[CrossRef](#)]
15. Hua, R.; Niu, J.; Chen, B.; Li, M.; Yu, T.; Li, W. Visible quantum cutting in GdF<sub>3</sub>:Eu<sup>3+</sup> nanocrystals via downconversion. *Nanotechnology* **2006**, *17*, 1642–1645. [[CrossRef](#)]
16. Chen, Y.; Liu, B.; Shi, C.; Kirm, M.; True, M.; Vielhauer, S.; Zimmerer, G. Luminescent properties of Gd<sub>2</sub>SiO<sub>5</sub> powder doped with Eu<sup>3+</sup> under VUV–UV excitation. *J. Phys. Condens. Matter* **2005**, *17*, 1217–1224. [[CrossRef](#)]
17. Wegh, R.T.; Donker, H.; Oskam, K.D.; Meijerink, A. Visible Quantum Cutting in LiGdF<sub>4</sub>:Eu<sup>3+</sup> Through Downconversion. *Science* **1999**, *283*, 663–666. [[CrossRef](#)]
18. Van der Kolk, E.; Dorenbos, P.; Krämer, K.; Biner, D.; Gudel, H. High-resolution luminescence spectroscopy study of down-conversion routes in NaGdF<sub>4</sub>:Nd<sup>3+</sup> and NaGdF<sub>4</sub>:Tm<sup>3+</sup> using synchrotron radiation. *Phys. Rev. B* **2008**, *77*, 125110. [[CrossRef](#)]
19. You, F.; Zhang, X.; Peng, H.; Huang, S.; Huang, Y.; Tao, Y. Energy transfer and luminescent properties of Pr<sup>3+</sup> and/or Dy<sup>3+</sup> doped NaYF<sub>4</sub> and NaGdF<sub>4</sub>. *J. Rare Earths* **2013**, *31*, 1125–1129. [[CrossRef](#)]
20. Hachani, S.; Guerrous, L. Synthesis, Luminescence, and Energy Transfer Properties of YPO<sub>4</sub>:Gd<sup>3+</sup>, Eu<sup>3+</sup> and YP<sub>3</sub>O<sub>9</sub>:Sm<sup>3+</sup>, Eu<sup>3+</sup> Phosphors. *J. Fluoresc.* **2019**, *29*, 665–672. [[CrossRef](#)]
21. Li, D.; Zhu, G.; Zhao, X. High efficiently color-tunable emission in KTb(CO<sub>3</sub>)<sub>2</sub>:Eu<sup>3+</sup> phosphors. *Opt. Mater.* **2021**, *119*, 111310. [[CrossRef](#)]
22. Li, D.; Zhu, G. Quantum Cutting in Ultraviolet B-Excited KY(CO<sub>3</sub>)<sub>2</sub>:Tb<sup>3+</sup> Phosphors. *Materials* **2022**, *15*, 6160. [[CrossRef](#)] [[PubMed](#)]
23. Lin, Y.; Hu, C.-L.; Fang, Z.; Chen, J.; Xie, W.-J.; Chen, Y.; Wang, J.-P.; Mao, J.-G. KRE(CO<sub>3</sub>)<sub>2</sub> (RE = Eu, Gd, Tb): New mixed metal carbonates with strong photoluminescence and large birefringence. *Inorg. Chem. Front.* **2022**, *9*, 5645–5652. [[CrossRef](#)]
24. Cao, L.; Peng, G.; Yan, T.; Luo, M.; Lin, C.; Ye, N. Three alkaline-rare earth cations carbonates with large birefringence in the deep UV range. *J. Alloys Compd.* **2018**, *742*, 587–593. [[CrossRef](#)]
25. Kutlu, I.; Kalz, H.-J.; Wartchow, R.; Ehrhardt, H.; Seidel, H.; Meyer, G. Kalium-Lanthanoid-Carbonate, KM(CO<sub>3</sub>)<sub>2</sub> (M = Nd, Gd, Dy, Ho, Yb). *Z. Anorg. Allg. Chem.* **1997**, *623*, 1753–1758. [[CrossRef](#)]
26. Shannon, R. Revised effective ionic radii and systematic studies of interatomic distances in halides and chalcogenides. *Acta Crystallogr. A* **1976**, *32*, 751–767. [[CrossRef](#)]

27. Carnall, W.T.; Fields, P.R.; Rajnak, K. Electronic Energy Levels of the Trivalent Lanthanide Aquo Ions. III.  $Tb^{3+}$ . *J. Chem. Phys.* **1968**, *49*, 4447–4449. [[CrossRef](#)]
28. Gómez-Morales, J.; Fernández-Penas, R.; Acebedo-Martínez, F.J.; Romero-Castillo, I.; Verdugo-Escamilla, C.; Choquesillo-Lazarte, D.; Esposti, L.D.; Jiménez-Martínez, Y.; Fernández-Sánchez, J.F.; Iafisco, M.; et al. Luminescent Citrate-Functionalized Terbium-Substituted Carbonated Apatite Nanomaterials: Structural Aspects, Sensitized Luminescence, Cytocompatibility, and Cell Uptake Imaging. *Nanomaterials* **2022**, *12*, 1257. [[CrossRef](#)]
29. Yang, Z.; Hu, Y.; Chen, L.; Wang, X. Color tuning of  $Ba_2ZnSi_2O_7:Ce^{3+},Tb^{3+}$  phosphor via energy transfer. *J. Lumin.* **2014**, *153*, 412–416. [[CrossRef](#)]
30. Halmurat, D.; Yusufu, T.; Wang, Q.-l.; He, J.; Sidike, A. Rare earth ion  $Tb^{3+}$  doped natural sodium feldspar ( $NaAlSi_3O_8$ ) Luminescent properties and energy transfer. *Sci. Rep.* **2019**, *9*, 14637. [[CrossRef](#)]
31. Zhou, W.; Zhang, W.; Yin, M. Study on spectroscopic properties of  $GdOBr:RE^{3+}$  (RE = Eu, Tb, Ce). *J. Rare Earths* **2008**, *26*, 459–462. [[CrossRef](#)]
32. Omanwar, S.K.; Jaiswal, S.R.; Sawala, N.S.; Koparkar, K.A.; Bhatkar, V.B. Ultra-violet to visible quantum cutting in  $YPO_4:Gd^{3+},Tb^{3+}$  phosphor via down conversion. *Mater. Discov.* **2017**, *7*, 15–20. [[CrossRef](#)]
33. Jaiswal, S.R.; Sawala, N.S.; Nagpure, P.A.; Bhatkar, V.B.; Omanwar, S.K. Visible quantum cutting in  $Tb^{3+}$  doped  $BaGdF_5$  phosphor for plasma display panel. *J. Mater. Sci. Mater. Electron* **2017**, *28*, 2407–2414. [[CrossRef](#)]
34. Xiong, H.; Zhang, Y.; Liu, Y.; Gao, T.; Zhang, L.; Qiao, Z.; Zhang, L.; Gan, S.; Huo, Q. Self-template construction of honeycomb-like mesoporous  $YPO_4:Ln^{3+}$  (Ln = Eu, Tb) phosphors with tuneable luminescent properties. *J. Alloy. Compd.* **2019**, *782*, 845–851. [[CrossRef](#)]
35. Zhang, D.; Li, G.; Yang, W.; Huang, W.; Leng, Z.; Fang, S.; Li, L. Tunable photoluminescence properties and energy transfer of  $Ca_5(BO_3)_3F:Tb^{3+}/Eu^{3+}$  phosphors for solid state lighting. *J. Lumin.* **2019**, *208*, 155–163. [[CrossRef](#)]
36. Li, M.; Wang, L.; Ran, W.; Deng, Z.; Shi, J.; Ren, C. Tunable Luminescence in  $Sr_2MgSi_2O_7:Tb^{3+},Eu^{3+}$  Phosphors Based on Energy Transfer. *Materials* **2017**, *10*, 227. [[CrossRef](#)]
37. Qiao, J.; Zhang, Z.; Zhao, J.; Xia, Z. Tuning of the Compositions and Multiple Activator Sites toward Single-Phased White Emission in  $(Ca_{9-x}Sr_x)MgK(PO_4)_7:Eu^{2+}$  Phosphors for Solid-State Lighting. *Inorg. Chem.* **2019**, *58*, 5006–5012. [[CrossRef](#)] [[PubMed](#)]
38. Yaiphaba, N.; Ningthoujam, R.S.; Singh, N.R.; Vatsa, R.K. Luminescence Properties of Redispersible  $Tb^{3+}$ -Doped  $GdPO_4$  Nanoparticles Prepared by an Ethylene Glycol Route. *Eur. J. Inorg. Chem.* **2010**, *18*, 2682–2687. [[CrossRef](#)]
39. Cao, J.; Chen, W.; Xu, D.; Li, X.; Wei, R.; Chen, L.; Sun, X.; Guo, H. Transparent glass ceramics containing  $Lu_6O_5F_8:Tb^{3+}$  nano-crystals: Enhanced photoluminescence and X-ray excited luminescence. *J. Am. Ceram. Soc.* **2018**, *101*, 1585–1591. [[CrossRef](#)]

**Disclaimer/Publisher’s Note:** The statements, opinions and data contained in all publications are solely those of the individual author(s) and contributor(s) and not of MDPI and/or the editor(s). MDPI and/or the editor(s) disclaim responsibility for any injury to people or property resulting from any ideas, methods, instructions or products referred to in the content.